Journal of Membrane Science 683 (2023) 121841

Contents lists available at ScienceDirect

Journal of Membrane Science

journal homepage: www.elsevier.com/locate/memsci

Gas adsorption isotherm, pore size distribution, and free volume fraction of polymer-polymer mixed matrix membranes before and after thermal rearrangement

C. Soto [a,b], N. Cicuttin [a], F.J. Carmona [a,b], M. de la Viuda [a,b], A. Tena [a,b], Á.E. Lozano [a,c,d], A. Hernández [a,b], L. Palacio [a,b,**], P. Prádanos [a,b,*]

[a] Surfaces and Porous Materials (SMAP), Associated Research Unit to CSIC, Universidad de Valladolid, Facultad de Ciencias, Paseo Belén 7, E-47011, Valladolid, Spain
[b] Institute of Sustainable Processes (ISP), Dr. Mergelina S/n, 47011, Valladolid, Spain
[c] Institute for Polymer Science and Technology (ICTP-CSIC), Juan de la Cierva 3, 28006, Madrid, Spain
[d] IU CINQUIMA, University of Valladolid, Paseo Belén 5, E-47011, Valladolid, Spain

ARTICLE INFO

Keywords:
CO_2 adsorption
N_2 adsorption
Free volume
Mixed matrix membranes
Porous polymer networks
Thermal rearrangement

ABSTRACT

In this work, CO_2 adsorption at 273.15 K and N_2 adsorption at 77 K of mixed matrix membranes has been studied, as a method to directly determine their fractional free volume (FFV). These membranes consist of a continuous phase of copoly(o-hydroxyamide)s (HPA) or copoly(*o*-hydroxyamide-amide)s (PAA) and a relatively highly porous polymer network filler (PPN1). Both the pure copolymers and the mixed matrix membranes (MMMs) have been analyzed before and after a thermal rearrangement (TR) process.

The CO_2 adsorption results have allowed characterizing the pore size distribution of the studied membranes in the 3–15 Å range, by using the Non-Local Density Functional Theory (NLDFT). Whereas the N_2 adsorption has allowed determining the pore size distributions in the range between 20 and 250 Å.

The experimental determination of the pore volume and the density allows the direct calculation of the membranes' free volume fractions, which were in good agreement with the most usual FFV evaluation methods. In addition, part of the pore volume detected by N_2 adsorption was associated with defects and poor integration of the membrane components. This correction has allowed us to make a new evaluation of the density of these materials.

1. Introduction

The importance of dense membranes has gone hand in hand with declining fossil fuel reserves and growing concern about climate change. This current work focuses on materials with good permeation properties and high selectivities, which allow us to concentrate and purify gases [1,2]. Although efforts are being made to improve conventional techniques such as cryogenic distillation [3], chemical adsorption [4], or amine absorption [5], their energy consumption is higher than those of membrane-based separation processes, which are more efficient and economical [6–9] whilst having a smaller carbon footprint.

The development of new materials for gas separations has followed various development paths. Among them, Mixed Matrix Membranes (MMMs) have emerged as a way to increase the efficiency of gas separation materials. These MMMs are the result of the addition of organic and/or inorganic materials (disperse phase) to a polymeric matrix (continuous phase) in order to form a hybrid material [10–15]. A wide variety of fillers and polymers have been made to improve the capabilities of these membranes and to increase their ability to perform well in aggressive environments and high temperatures [16,17]. On the other hand, it has been seen that certain heat treatments have also improved the properties of such materials. In this sense, some thermally rearranged (TR) polymers have emerged as promising materials for gas separation due to their outstanding performance [18]. Polymers and

* Corresponding author. Surfaces and Porous Materials (SMAP), Associated Research Unit to CSIC, Universidad de Valladolid, Facultad de Ciencias, Paseo Belén 7, E-47011, Valladolid, Spain.
** Corresponding author. Surfaces and Porous Materials (SMAP), Associated Research Unit to CSIC, Universidad de Valladolid, Facultad de Ciencias, Paseo Belén 7, E-47011, Valladolid, Spain.
E-mail addresses: laura.palacio@uva.es (L. Palacio), ppradanos@uva.es (P. Prádanos).

https://doi.org/10.1016/j.memsci.2023.121841
Received 26 April 2023; Received in revised form 2 June 2023; Accepted 10 June 2023
Available online 16 June 2023

copolymers, such as ortho-hydroxy polyimides and polyamides, capable of producing poly-1,3-benzoxazoles (PBO) when subjected to a thermal rearrangement have been used as the polymeric matrix to manufacture TR-MMMs. Other related TR polymers are polybenzothiazoles (PBZ), polypyrrolone (PPL), depending on the functional groups placed at the *ortho* position of an amione group [19,20]. Interesting results have been found with PIOFG-1, synthesized from 4,4'-(hexafluoroisopropylidene)-diphthalic anhydride (6FDA) and 2,2′-bis(3-amino-4-hydroxylphenyl) hexafluoropropane (bisAPAF) via thermal imidization above 300 °C [21]. Also 3.3′-diamino-4.4′-dihydroxybiphenyl (mHAB), which is an isomeric monomer of commercial 3.3′-dihydroxybenzidine (HAB), having a *meta* diamine moiety [22] wass combined with2,2-bis(3-amino-4-hydroxy-phenyl) hexafluoropropane (bisAPAF), 4,4-oxydianiline (ODA), and 3,3,4,4-biphenyltetracarboxylic dianhydride (BPDA), which drived to TR-PBO-co-PI (TR poly(benzoxazole-co-imide)) with CO_2 permeabilities higher than 1000 Barrers [23]. The formations of copolymers, like this last example, can also improve the mechanical properties of the TR-membranes.

The permeation mechanisms of those materials can be linked to the fractional free volume (FFV). A polymer with a high FFV causes significant inter-chain separation thus, increase permeability and give greater size selectivity if the polymer chain rigidity is increased what subsequently improves the solubility selectivity [24]. Therefore, FFV is among the most important structural variables influencing gas transport properties in polymers [25,26], because it is directly related with diffusion coefficients as the Cohen-Turnbull model predicts [27]. Different efforts have been made to increase FFV. Apart from the aforementioned TR treatment, some materials have been designed with this objective in mind. For example, polymers with intrinsic microporosity (PIMs [19,28,29]) or fillers as zeolite [30], carbon materials [31] and metal organic frameworks (MOFs [32,33]).

Several methods to calculate FFV are available. Some of them are theoretical in nature and involve the evaluation of the occupied volume of the polymer; this can be determined via the Bondi group contribution method [34,35]. Subsequently, Van Krevelen [36] developed the group contribution methodology to evaluate the van der Waals volume of a polymer. Through the years, different modifications and discussions arose [37]. More recently, Van der Waals volumes have been determined from the geometry optimization of the structural unit obtained by quantum DFT or semi-empirical methods [38], finding the value of the volume using a computer numerical integration method. Other software packages, as BIOVIA Materials Studio [39] use values from adsorption processes via Grand Canonical Monte Carlo (GCMC) method in adsorption simulation.

Positron annihilation lifetime spectroscopy (PALS) also allows an estimation of fractional free volume as $FFV = N \cdot v_F$, where N is the hole number density (concentration of holes) and v_F is the mean volume of the spherical hole with the radius R in the polymer or $v_F = 4/3(\pi R^3)$. The FFV values found in this manner are usually smaller than FFV estimated via Bondi groups contribution methods by a factor 3–4 [40–42].

Other experimental approaches can be used to obtain data for the FFV evaluation. For example Soto et al. [18,43] have shown that FFV can also be evaluated from measurements of permeability, based on previous works of Thornton et al. [44]. Other methods [45] include inverse gas chromatography (IGC [46]), ^{129}Xe NMR spectroscopy [47], electrochromic [48] analysis, spin probe tests, or photochromic probe methods [49].

In this work, a deep analysis of FFV of promising MMMs and their corresponding TR-MMMs, which were obtained and characterized by us [18,50] has been performed, from adsorption-desorption measurements of CO_2 and N_2. The originality of this work relies on the use of a conventional and easily accessible technique to obtain a parameter that can quickly predict the performances of our materials for gas separation processes.

2. Experimental

2.1. Materials

Here the porosity of some copolyamides, derived from the combination of TR-able diamines (4′4-propane-2,2-diylbis(2-aminophenol), APA, 2,2-bis(3-amino-4-hydroxyphenyl)hexafluoroisopropylidene, APAF) and non-TR-able diamines (4,4'-(hexafluoroisopropylidene)dianiline, 6FpDA) with the dichloride 2,2-bis(4-chlorocarbonylphenyl)hexafluoropropane (6FCl), will be studied by adsorption desorption methods. These copolyamides—copoly-o-hydroxyamide (APAF-APA-6FCl) and copoly-o-hydroxyamide-amide (APAF-6FpDA-6FCl)—will be referred to as HPA and PAA, respectively. The corresponding MMMs, and thermally rearranged MMMs, TR-MMMs, resulting from the mixture of the resulting copolyamides with a triptycene-isatin Porous Polymer Network, PPN1, as a filler, will also be studied. Thermal rearrangement was performed in a ceramic furnace in a N_2 atmosphere. The procedure applied was based on previous TGA studies that showed a maximal conversion for both the copolymers at 375 K, specifically 91% for HPAs and 96% for PPAs [18]. In Fig. 1, the structures are schematically shown and in Table 1 the corresponding nomenclature used here is shown. These MMMs and TR-MMMs were previously studied by us, attending to their gas separation features [18].

For gas adsorption-desorption measurements, nitrogen, and carbon dioxide, with high purity (>99.999), were used. Helium was used as backfill gas and for chamber volume calibration. In the case of nitrogen adsorption isotherms at 77 K, liquid nitrogen was used to reach this temperature. All products have been supplied by Air Liquide company.

2.2. Characterization

Pore characterization was carried out in a volumetric device Autosorb IQ (Quantachrome Instruments). Samples were degassed at 100 °C for 10 h under vacuum, before the sorption measurements, to eliminate possible adsorbed gases or water vapour. The adsorption isotherm data were used to obtain the pore size distribution by the non-local density functional theory equilibrium model (NLDFT). Acquisition and calculation were carried out by Quantachrome® ASiQwin software (version 5.21).

For all the samples detailed in Table 1, and the pure filler PPN1 (triptycene-isatin Porous Polymer Network), the adsorption isotherms have been measured first for CO_2 at 273.15 K (up to $p/p_0 = 0.03$), afterwards with N_2 at 77 K (up to $p/p_0 = 1$) and finally again with CO_2 at 273.15 K. The minimum time kept in equilibrium for each point was 300 s to be sure to get complete diffusion [51] and constant adsorbed gas as tested. For the sake of analyzing the influence of temperature on the CO_2 adsorption process, the isotherms at 269.75 K, 273.15 K, 293.15, 303.15 K and 308.15 K have been measured for samples of the TR-HPA membrane.

The skeletal volume of PPN1 has been determined with an AccuPyc 1330 V2.04 N (Micromeritics Instrument Corporation, Norcross, GA, USA), as previously described by the authors [18].

Densities of the samples detailed in Table 1, have been measured according to the Archimedes principle in a CP225 Analytical Balance from Sartorius (Sartorius, Göttingen, Germany) equipped with a density measurement kit. The samples were weighed in air and into high pure isooctane at room temperature. The average density from seven samples was obtained as:

$$\rho^i = \rho_{C_8H_{18}} \frac{W_{air}}{W_{air} - W_{C_8H_{18}}} \qquad i = MMM, F \text{ or } M \tag{1}$$

Here $\rho_{C_8H_{18}}$ corresponds to the isooctane's density, W_{air} corresponds to the sample weight and $W_{C_8H_{18}}$ stands for the weight of the sample when

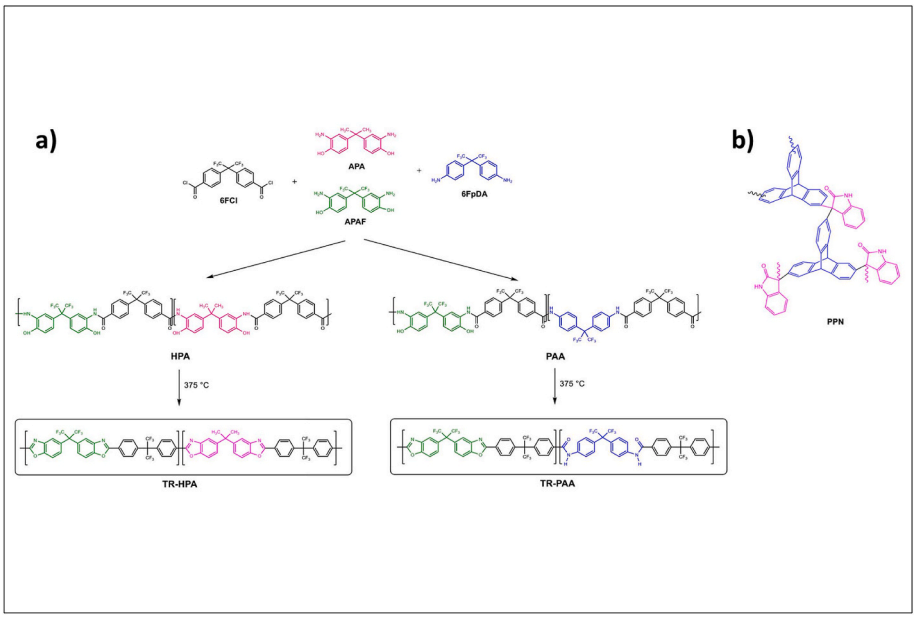

Fig. 1. a) Scheme of the polymerization of copoly-o-hydroxyamides and copoly-o-hydroxyamideamide and their transformation by thermal rearrangement. b) Structure of the PPN derived from triptycene and isatin [18].

Table 1
Nomenclature of the studied membranes. xx represent the percent of PPN1 in the membrane, TR denotes thermally rearranged membranes, and HPA and PAA indicate that the MMMs is manufactured from o-hydroxipolyamides or o-hydroxypolyamides-amides respectively.

Continuous phase	Neat membranes	TR-PBO
Copoly-o-hydroxyamide-amide (APAF-6FpDA-6FCl)	PAA	TR-PAA
	PAAxx	TR-PAAxx
Copoly-o-hydroxyamides (APAF-APA-6FCl)	HPA	TR-HPA
	HPAxx	TR-HPAxx

submerged in isooctane.

3. NLDFT method

In the last 70 years, the development of reliable methods for the elucidation of porosity in activated carbons and other porous materials has been the focus of numerous research efforts [52].

For years, phenomenological models of adsorption based on Dubinin's theory [53] of volume filling of micropores have found great utility in describing the adsorption equilibrium of various gases and vapors. More recently, advances in molecular modeling of adsorption phenomena by means of Monte Carlo simulations [54] and density functional theory, DFT, calculations have led to a better understanding of the specifics of interactions of adsorbed species with porous carbon [55,56].

The relation between isotherms determined by these microscopic approaches and the experimental isotherm on a porous solid can be interpreted in terms of a *Generalized Adsorption Isotherm (GAI)* equation:

$$N_{exp}(p/p_0) = \int_{W_{min}}^{W_{Max}} N(p/p_0, W) f(W) dW \tag{2}$$

where $N_{exp}(p/p_0)$ is the experimental adsorption isotherm data, W is the pore width, $N(p/p_0, W)$ is the isotherm on a single pore of width W and $f(W)$ is the pore size distribution function.

The GAI equation reflects the assumption that the total isotherm consists in a number of individual *single pore* isotherms multiplied by their relative distribution, $f(W)$, over a range of pore sizes. The set of $N(p/p_0, W)$ isotherms (kernel) for a given system (adsorbate/adsorbent) can be obtained by either Density Functional Theory (our case) or by Monte Carlo computer simulation. The pore size distribution is then derived by solving the GAI equation numerically via a fast non-negative least square algorithm.

The adsorption experiment collects solid–fluid (adsorbent–adsorbate) s equilibrium states at a given temperature and a set of adsorbate gas pressures, corresponds to the conditions of the grand canonical ensemble for the system of fixed chemical potential μ, volume V, and temperature T. Therefore, the equilibrium distribution of the adsorbate in the pores corresponds to a minimum of the grand potential $\Omega(T, V, \mu)$ of the adsorption system presented as a functional of the density of adsorbed fluid.

We assume that in adsorption, the solid adsorbent is inert and non-deformable, and the adsorption interactions are modeled with an effective solid–fluid spatially distributed potential $U_{ext}(\boldsymbol{r})$. In these conditions, the equilibrium adsorption state at a given chemical potential of the fluid μ_f is determined by the minimization of the *grand potential* Ω_f of the fluid confined in the pore and subjected to the external potential $U_{ext}(\boldsymbol{r})$ [57,58]:

$$\Omega_f[\rho_f(\boldsymbol{r})] = F_f[\rho_f(\boldsymbol{r})] - \int \rho_f(\boldsymbol{r})[\mu_f - U_{ext}(\boldsymbol{r})]dr \tag{3}$$

where $\boldsymbol{r}$ is a position vector inside the pore, $\rho_f(\boldsymbol{r})$ is the fluid density, and F_f is the Helmholtz free energy of the fluid. F_f is the sum of the ideal ($F_{id}[\rho_f(\boldsymbol{r})]$) and excess ($F_{ex}[\rho_f(\boldsymbol{r})]$) components of the Helmholtz free energy of the reference hard-sphere (HS) fluid and the attractive term calculated from the fluid-fluid intermolecular potential ($u_{ff}(\boldsymbol{r})$), treated in a mean-field fashion given by the equation:

$$F_f[\rho_f(\boldsymbol{r})] = F_{id}[\rho_f(\boldsymbol{r})] + F_{ex}[\rho_f(\boldsymbol{r})] + \frac{1}{2}\iint \rho_f(\boldsymbol{r})\rho_f(\boldsymbol{r}')u_{ff}(|\boldsymbol{r}-\boldsymbol{r}'|)d\boldsymbol{r}d\boldsymbol{r}' \quad (4)$$

The Lennard-Jones (LJ) potential can be used to model fluid-fluid interactions, according to the Weeks-Chandler-Andersen (WCA) scheme [59]:

$$u_{ff}(\boldsymbol{r}) = 4\varepsilon_{ff}\left[(\sigma_{ff}/r)^{12} - (\sigma_{ff}/r)^{6}\right] \quad (5)$$

where ε_{ff} and σ_{ff} are the well depth and distance parameters of the LJ potential.

Minimizing the grand potential (Eq. (3)), the fluid density profile $\rho_f(\boldsymbol{r})$ is obtained, according to the Euler-Lagrange equation:

$$\rho_f(\boldsymbol{r}) = \Lambda^{-3}\exp\left\{c(\boldsymbol{r},[\rho]) - \beta\int \rho_f(\boldsymbol{r})u_{ff}(|\boldsymbol{r}-\boldsymbol{r}'|)d\boldsymbol{r}' + \beta\mu - \beta U_{ext}(\boldsymbol{r})\right\} \quad (6)$$

where $c(\boldsymbol{r},[\rho]) = -\beta\delta F_{ex}[\rho_f(\boldsymbol{r})]/\delta\rho_f(\boldsymbol{r})$ is one-particle direct correlation function expressed as the functional derivative of the excess Helmholtz free energy of the HS fluid, Λ is the de Broglie wavelength, and $\beta = 1/k_BT$. The HS term $c(\boldsymbol{r},[\rho])$ is taken from Tarazona's smoothed density approximation (SDA) [60,61]. More explicit equations can be found in the literature elsewhere [62–64].

Once the equilibrium distribution of the fluid density is determined at each value of the chemical potential μ_f, and its averaged values calculated, the adsorption isotherm can be obtained as:

$$N(p/p_0, W) = \frac{1}{2}\left(\int_0^{W_{cc}} \rho_f(\boldsymbol{r})d\boldsymbol{r} - \rho_{bulk}(p/p_0)W_{ref}\right) \quad (7)$$

where $\rho_{bulk}(p/p_0)$ is the bulk density, and W_{ref} is a reference pore width, which here we took to be equal to the internal pore width: $W_{ref} = W = W_{cc} - \sigma_{cc}$, using $\sigma_{cc} = 3.4$ Å for the effective diameter of the carbon atom. In principle, to be fully consistent with experimental practice one should use W_{ref} obtained from the theoretical helium calibration performed at the same conditions as the experimental determination of the void volume [65]. For CO_2 adsorption at high pressures, we used theoretical absolute adsorption isotherms, because the experimental isotherms we used have already been converted from excess to absolute adsorption [66]. Thus, effects of He adsorption were neglected.

4. Free volume fractions

The most common method used to evaluate the free volume fraction can be described as follows:

$$FFV = \frac{V - V_0}{V} \quad (8)$$

Here $V = 1/\rho$ (ρ being the density) and V_0 is the volume of the chain per unit mass. V_0 can be obtained from the van der Waals [34,35,37] specific volume, V_w, as:

$$V_0 = 1.33\cdot V_w \quad (9)$$

The van der Waals volume can be evaluated by using the Bondi's group contribution theory [36] or by methods based on molecular modeling of the polymer repeating units, with programs like Hyperchem Molecular Modeling [67,68] or BIOVIA Materials Studio [39,50], as we mentioned before.

For the case of MMMs and assuming non-interacting perfect integration between the matrix and the filler, we can calculate the *FFV* as:

$$FFV^{MMM} = \varphi_V FFV^F + (1-\varphi_V)FFV^M \quad (10)$$

Here φ_V being the volume fraction of the filler in the MMM. FFV^F and FFV^M are the FFV of the filler and the polymeric matrix, respectively, evaluated according to Eqs. (8) and (9). The filler specific volume can be evaluated as the sum of its skeletal specific volume V_{sk}^F plus the specific volume within the filler pores V_p^F:

$$V^F = V_{sk}^F + V_p^F \quad (11)$$

V_{sk}^F is measured by gas pycnometry and V_p^F by CO_2 adsorption at 273 K. The densities (or specific volumes) of the pure polymers and their TRs were determined by the Archimedes method, as mentioned in section 2.2.

This work proposes the FFV determination of these MMMs from direct experimental measurements as:

$$FFV = \frac{V_{ads}}{V^{MMM}} \quad (12)$$

Here $V^{MMM} = 1/\rho^{MMM}$ and V_{ads} is the CO_2 adsorbed volume per unit of mass as measured by adsorption. The choice of CO_2 as adsorbate for the determination of the free volume is based on its small size, its high affinity for this type of materials (ensuring its penetrability) and its critical temperature above 30 °C (ensuring condensation under the measurement conditions).

Recently [43,50] we proposed and validated a correlation between permeability and free volume, as:

$$P = Ae^{B\cdot FFV} \quad (13)$$

with $B = a + b\delta + c\delta^2$. Thus:

$$\ln P = [\ln A + a\cdot FFV] + [b\cdot FFV]\delta + [c\cdot FFV]\delta^2 \quad (14)$$

Here, δ is the kinetic diameter of the tested gas, and A, a, b and c are constants that, in principle, should be independent of the load. Using this correlation for different gases we evaluated the FFV determining permeability [18].

5. Results and discussions

5.1. Gas adsorption and pore size distribution

The adsorption isotherms for CO_2 show that the amount of gas adsorbed increases with the amount of filler included, being for the pure PPN1 higher than for all mixed matrix membranes. In Fig. 2 some examples of the MMMs, before and after thermal rearrangement, of both PAAs and HPAs families are shown. In all cases, the isotherms correspond to the I type within the IUPAC classification [52], which is the expected adsorption within micropores.

The N_2 adsorption-desorption isotherms at 77 K were performed with the same membranes as CO_2 adsorption isotherms (an example is shown in Fig. S1 in the supplementary documentation). All cases present a hysteresis loop, with very similar shapes that would correspond to microporous interconnected materials. The appearance of such hysteretic loops at low pressures would indicate the presence of swelling and/or restricted diffusional access to narrow micropores [51]. For N_2 adsorption there is not any correlation between the adsorbed amount and the filler load. This can be due to the presence of apparently randomly appearing interstices between the PPN1 filler and the polymeric matrix or, even, to holes, bubbles, breaches, etc, appearing within the polymeric matrix itself. Some of these imperfections can be seen in SEM pictures of transversal cuts of these membranes previously published by us [18]. Note that the amount of N_2 adsorbed is sensibly lower than the amount of CO_2 (compare Fig. 2 and S1).

Because we are dealing with polymeric chains and networks, both for the matrix and the filler, the interstices would constitute micropores, as confirmed for PPN1 by Lopez-Iglesias et al. [51] Attending to the similarities of the adsorption isotherms for PPN1 and the MMMs both for N_2 and CO_2, the non-local density functional theory (NLDFT) method appears as the most appropriate alternative to obtain the pore size

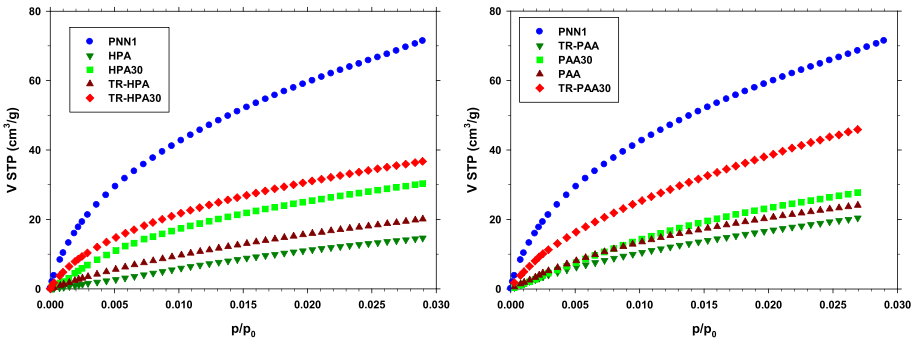

Fig. 2. Adsorption isotherms for CO_2 at 273.15 K for PPN1 and some of the mixed matrix membranes of the HPAs (left) and PAAs (right) series, both before and after thermal rearrangement.

distributions for these materials. The reason is because the free volume is formed by the space between the polymer chains, which can be assimilated to a network of interconnected slit-like pores. However, it has been probed that other approaches that consider the interactions of the gas with different polymer molecules such as the already mentioned GCMC method, applicable to the same range of pores, in the case of CO_2 gives very similar results. Nevertheless, in our case, the NLDFT method errors were always smaller than for GCMC. Moreover, a comparative study of the different models applicable to the systems analyzed in this work shows that the NLDFT is the most convenient (see Fig. S2 in the supplementary material).

The pore size distributions for CO_2 at 273.15 K shows the presence of pores within the entire range where the NLDFT theory is applicable (from 3 to 15 Å). In Fig. 3, we see that PPN1 gives three peaks with clear maxima in 3.5 Å, 5.26 Å, and 8.24 Å. The pure polymeric matrices and the MMMs show more complex distributions as shown in Fig. 3 for HPA and HPA30 before and after thermal rearrangement. PAA both before and after thermal rearrangement (see Figs. S3a and S3b in the supplementary information) show similar behavior.

It is seen that pore sizes are always distributed within the same three intervals around 3.5 Å, 5.26 Å and 8.24 Å, except for the membranes of pure continuous polymeric matrices and without thermal rearrangement, which do not show the 3.5 Å peak. Moreover, the peaks around 3.5 Å are low for the corresponding MMMs, probably because these narrow pores could not be completely evacuated prior to the CO_2 adsorption, even for long vacuuming times. This could be due to the low diffusivity of the polymer that would decrease the effective pressure gradient. This could explain why they were not detected within HPA neither in PAA. This 3.5 Å peak appears for TR-HPA and TR-PAA, probably because thermal rearrangement increases diffusivity and accessibility allowing a better evacuation of these narrow pores and making them accessible for CO_2. Moreover, increasing amounts of PPN increase the defects within the polymeric matrix and decreases the paths that the gas must travel to be evacuated, allowing the detection of smaller pores.

Thermal rearrangement generates pores with a significant volume around the size of 3.5 Å for both PAA and HPA. In all cases, the relevance of this population of small pores increases with the PPN1 load. For TR-HPA, the peak is wider than for PPN1 and for TR-HPA30 it appears split between two peaks. This widening process do not appear for TR-PAA (see Fig. S3).

The rest of the peaks for HPA and PAA as well as their MMMs, both before and after thermal rearranging, correspond to volumes smaller than appearing for PPN1. It is noteworthy that the corresponding pore volume also increases after thermal rearrangement. A quantitative analysis of the area below the pore size distributions allows us to confirm

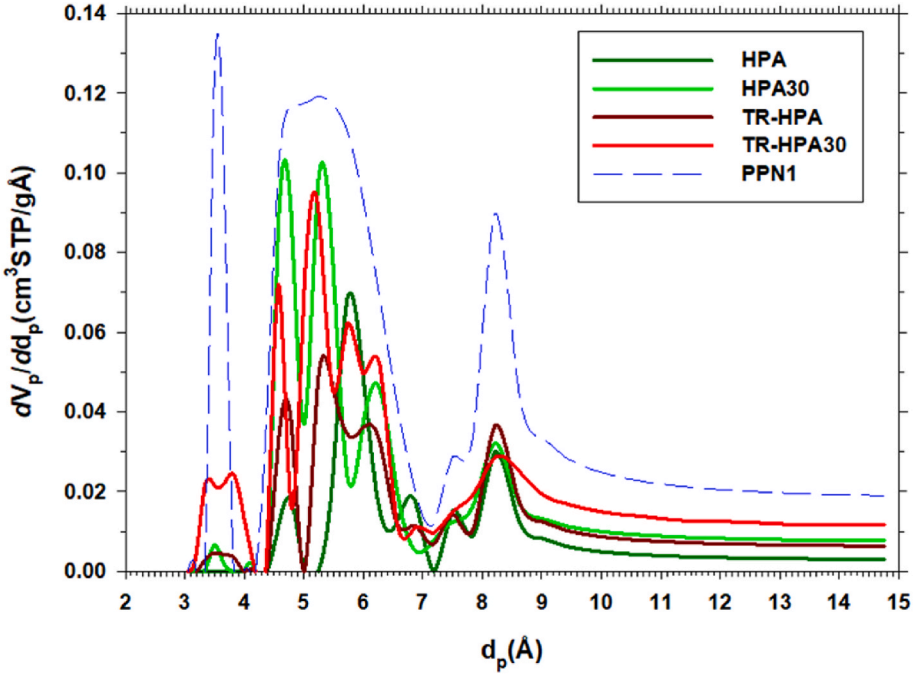

Fig. 3. Pore size distribution obtained from CO_2 isotherms (273.15 K) by the NLDFT method for PPN1 and HPA series before and after thermal rearrangement.

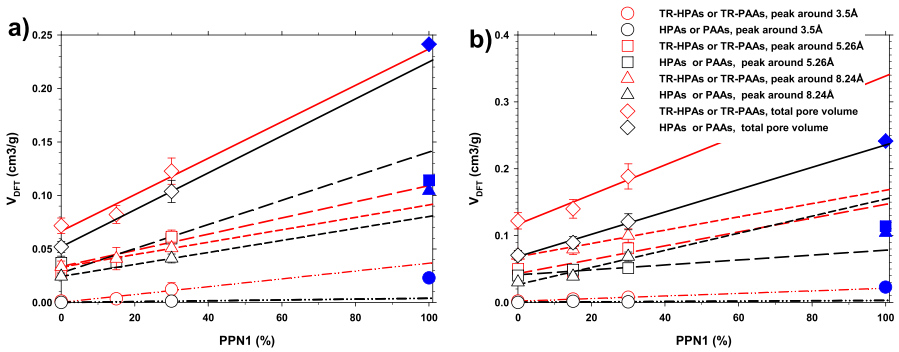

Fig. 4. Evolution of the pore volume for the three size ranges (centered on 3.5 Å, 5.26 Å and 8.24 Å), for the HPA a) and PAAs b) membranes, versus PPN1 loads. Extrapolation to 100% PPN1 content is in concordance with the experimental pore volumes for pure PPN1 (blue solid symbols). (For interpretation of the references to colour in this figure legend, the reader is referred to the Web version of this article.)

this tendency as shown in Fig. 4 for both the copolymer families. Within the error range, both the HPA and PAA, extrapolate approximately to the value for the pure PPN1.

The deviations between samples of the same manufacture batch are negligible whereas for different batches these deviations increase slightly especially for MMMs (see Fig. S4 in the supplementary material). The presence of higher batch-to-batch deviations could mean that the variability is mostly caused by the MMMs formation, being these differences more evident for N_2 adsorption.

To get quantitative information on porosities, the pore frequencies for the three size ranges (1st peak 3.1–4.2 Å, 2nd peak 4.2–7.2 Å and 3rd peak 7.2–15 Å) have been fitted to a Gaussian function. In Fig. 5, the case for HPA30 and TRHPA30 is shown. The equivalent figure for PAA is shown in Fig. S5 in the supplementary material. In both figures, we included the Power Spectral Density showing the chain *d*-spacing frequencies as obtained from wide angle x-ray scattering, WAXS [18]. In all cases, there is a chain *d*-spacing local maximum around 3.5 Å. The *d*-spacing for the first peak of HPAs is 3.66 ± 0.22 Å, and for TR-HPA it is 3.69 ± 0.25 Å. For PAA the *d*-spacing is 3.39 ± 0.04 Å and 3.42 ± 0.08 Å for the TR-PAA. These maxima in *d*-spacing could be in correspondence with the most probable polymer chain interstices or pores. The existence of such *d*-spacing even when, for the low permeability cases (non-TR without PPN1 membranes), it was not possible to detect any pores of this size by CO_2 adsorption, allows to hypothesize that they could be there, although possibly not accessible to adsorption.

In Fig. 5 it is seen that the 1st and 2nd peaks are more symmetric, while the 3rd one has a long tail (closer to that of a log-normal distribution). It can be noted as well, that the PPN1 distribution is quite akin to that of the MMMs as already observed in Fig. 3. The resulting mean, μ, and standard deviation, σ, of the fitted gaussians are shown in Table 2.

In Fig. 5 (Fig. S5, in the supplementary information, for the PAA membranes), the nominal size of the CO_2 molecule (3.30 Å [69]), is shown by a red vertical line. This size is close to, but lower than, the maxima for the 1st peak in all cases. Therefore, the 1st peak would control diffusivity, while the 2nd and 3rd peaks would be more responsible for solubility. This 1st peak has equal μ and σ for the membranes without thermal rearrangement, and for the pure PPN1 too. This would mean that this peak should be attributed to the filler. In all cases, the thermal rearrangement, and the increase in the filler load, increase both μ and σ in accordance with the corresponding increase of permeability [18] as can be seen in Figs. 6 and 7.

The mean value for the 2nd peak is quite similar for all the samples while σ increases for thermal rearrangement results. These peaks correspond to the more outstanding peak of chain segment lengths as detected by WAXS. WAXS gives maxima in *d*-spacing for this 2nd peak that show similar tendencies to those for the 1st peak (HPAs 5.75 ± 0.07

Table 2
Mean value, μ, and standard deviation, σ, for the Gaussians fitted for the three peaks obtained from CO_2 adsorption (273.15 K) for the membranes studied.

Parameters of the fitted gaussian μ±σ(Å)			
	1st peak	2nd peak	3rd peak
PNN1	3.57 ± 0.04	5.38 ± 0.75	7.53 ± 4.68
HPA		5.82 ± 0.68	8.25 ± 0.55
HPA30	3.57 ± 0.04	5.21 ± 0.65	8.23 ± 0.27
TR-HPA	3.59 ± 0.15	5.60 ± 0.74	6.69 ± 4.51
TR-HPA15	3.61 ± 0.22	5.48 ± 0.72	8.22 ± 4.50
TR-HPA30	3.64 ± 0.28	5.45 ± 0.71	8.49 ± 4.50
PAA		5.71 ± 0.64	8.38 ± 0.74
PAA15	3.57 ± 0.04	5.49 ± 0.69	8.14 ± 0.40
PAA30		5.66 ± 0.56	8.35 ± 0.14
TR-PAA	3.57 ± 0.10	5.56 ± 0.78	7.56 ± 4.31
TR-PAA15	3.58 ± 0.21	5.51 ± 0.77	8.38 ± 4.00
TR-PAA30	3.58 ± 0.16	5.44 ± 0.83	8.57 ± 4.06

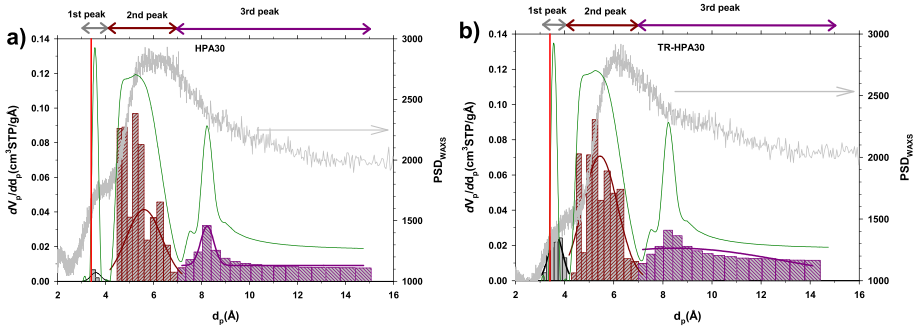

Fig. 5. Pore size distribution (bars) and their fitted Gaussians, for HPA30 (a) and TRHPA30 (b). The red vertical line corresponds to the size of the CO2 molecule, whereas the green curve is the pore size distribution for pure PPN1. The gray noisy curve corresponds to chain spacing obtained from WAXS. (For interpretation of the references to colour in this figure legend, the reader is referred to the Web version of this article.)

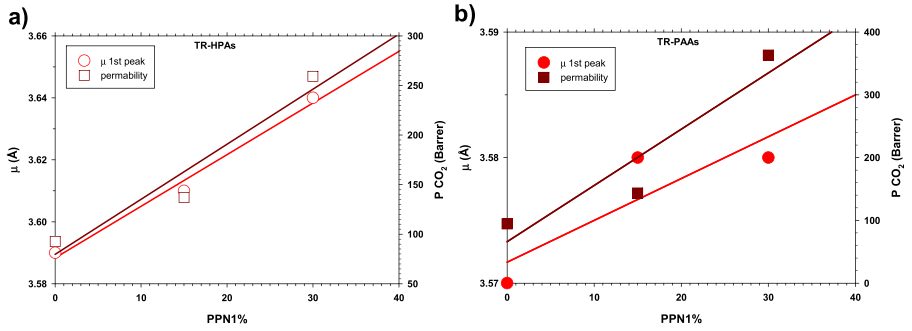

Fig. 6. Mean value, μ, for the first peak and permeability as a function of the PPN1 content for the TR-HPA (a) and TR-PAA (b) membranes. The lines correspond to linear fittings performed to simply show the existence of a monotonous tendency for μ to increase with the PPN1%.

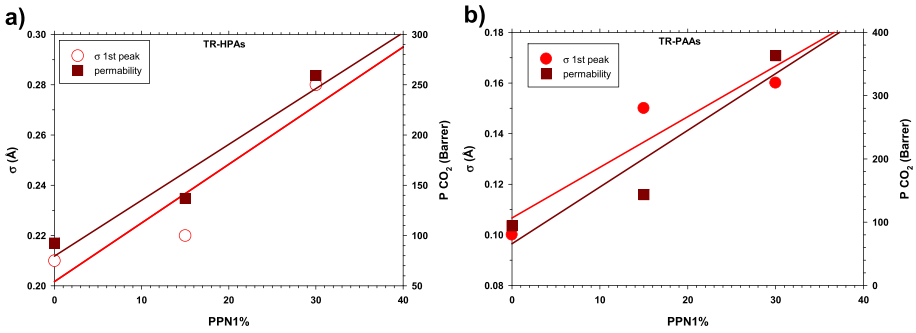

Fig. 7. Standard deviation, σ, for the first peak and permeability as a function of the PPN1 content for the TR-HPA (a) and TR-PAA (b) membranes. The lines correspond to linear fittings performed to simply show the existence of a monotonous tendency for σ to increase with the PPN1%.

Å, TRHPAs 5.95 ± 0.07 Å, PAAs 5.27 ± 0.06 Å and TRPAAs 5.47 ± 0.06 Å) [18]. Something similar is observed with the adsorption results when the third peak is analyzed.

In all cases, it is worth noting that WAXS results give always very wide and overlapping distributions. This is why it is difficult to correlate *d*-spacing with the content of filler in the MMMs.

N_2 adsorption can also be used to obtain the corresponding pore size distribution. These data can be treated by the NLDFT methodology as well because it gives also more detailed distributions. However, the Dubinin Astakhov (DA) [70] or Barrett-Joyner-Halenda (BJH) [71] methods give similar results (see Fig. S2 in supplementary material). The NLDFT method can be used for N_2 at 77 K assuming slit-like pores within the range from 3.5 to 400 Å. In our case, we only detected pores over 20 Å and below 250 Å. This can be seen in Fig. 8 for the HPA membranes, both before and after thermal rearrangement (the equivalent plot for the PAA membranes can be seen in Fig. S6 in the supplementary information). The distributions are similar for all the membranes studied, and for the pure PPN1 as well, and are clearly log-normal distributions. They show a maximum around 30 Å with a slow decay to wider pores. The distributions also depend strongly on the batch used as was the case for the CO_2 adsorption ones (see Figs. S4 and S7 in the supplementary information).

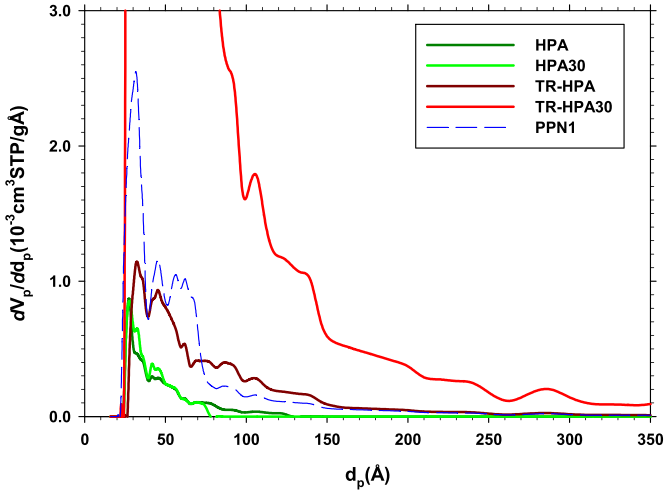

Fig. 8. Pore size distributions from N_2 adsorption at 77 K for the pure PPN1, HPA, their MMMs, and the thermally rearranged ones.

In some cases, see Fig. 8, the area under the curve (volume of pores) is higher than for the pure PPN1. This was also seen for the CO_2 adsorption as shown in Fig. S3 (in the supplementary information) for the PAA membranes and the third peak there. This can be due to the batch-to-batch variability, although it could be also due to the presence of interstitial spaces, created during the manufacture, between the continuous phase and the porous filler. It is important to note that in all cases the total porous volume obtained from N_2 adsorption is much smaller than that evaluated from CO_2 adsorption. In average, this porous volume from CO_2 adsorption is 200% that evaluated from N_2 adsorption for PAA and TR-PAA membranes and 500% in the case of the HPA and TR-HPA membranes. This seems to indicate that N_2 cannot enter the smaller pores so easily as CO_2. This should be due to smaller size of CO_2 (3.30 Å as compared to 3.64 Å for N_2 [69]), but it could also be due to a lower affinity of N_2 towards the polymeric matrix and filler. The estimation of the characteristic energy of adsorption, using the Dubinin Astakhov (DA) method, shows that it is more than an order of magnitude higher for CO_2 than for N_2 (see Table S1), which corroborates the lower affinity of N_2 for the polymer. An irreversible collapse of the fine porous structure could also happen at 77 K and should explain the absence of these small size pores when using N_2 isotherms. To investigate this possibility, measurements of porous volumes were performed with CO_2 at 273.15 K before and after measurements of adsorption of N_2 to 77 K. The differences were below 2.5% for PAA and TR-PAA membranes and

below 5% for the HPA and TR-HPA membranes. This allows discarding any irreversible structural collapse as a relevant factor.

The use of CO_2 adsorption isotherms at 273.15 K to determine the pore volume and its size distribution in microporous materials has become a standard method. However, the amount of adsorbed gas strongly depends on the temperature. In order to analyze this influence, measurements were made above and below 273.15 K (from 269.15 K to 308.15 K), with one of the samples studied in this work; one of them exceeding the critical temperature of 304.13 K. It is observed that the distributions are very similar for all temperatures, but above 273.15 K, in the case of pore sizes larger than 7 Å, part of the CO_2 condensation capacity is lost (see Fig. S8 in the supplementary material). As expected, the total volume of gas condensed in the pores also decreases with temperature. However, at 273.15 K and below, the value stabilizes, indicating that all the pores that the NLDFT method can determine are in effect totally filled (see Fig. S9 in the supplementary material).

The measurements of adsorption isotherms at different temperatures makes it possible to determine the isosteric heat of adsorption [72] ($q_{asd} = -\frac{dlnp}{d(\frac{1}{RT})}$) for CO_2. In our case, for TR-HPA simple, we have obtained a mean value of 15 ± 4 kJ/mol (see Fig. S10 in the supplementary material). This is more than two times its vaporization heat at the measurement temperature (6.52 kJ/mol at 288.95 K [73]), which means that there is a strong energetic interaction between CO_2 and our MMMs.

5.2. Free volume fractions, FFV

With the aim of evaluating the fractional free volume, the fractures and fissures coming from the matrix-filler mixing must not be contemplated. These big fracture interstices do not contribute to permeability by diffusion and solubility. We need to focus on the pores within the 3 Å to 15 Å that were detected by CO_2 adsorption. The pores detected by N_2, from 20 Å to 250 Å, would allow Knudsen flux corresponding to macroscopic features of these wider paths. Their effect on permeability would introduce random effects due to the intrinsically incontrollable (undesirable as well) nature of the manufacturing processes, that are susceptible to introduce interfacial imperfections. Moreover, the volume of the pores detected by CO_2 is 2–5 times greater than that corresponding to the pores detected by N_2, what allows to assume that the influence of the wider pores in the evaluation of FFV is lower.

In Fig. 9, the values of FFV obtained from van der Waals volume and from CO_2 adsorption measurements by Eqs. (10) and (12), respectively, are shown. Nevertheless, in both cases, the density used to get the specific volume should be corrected. In effect the density has been measured by using a procedure based on the Archimedes principle. This means that cracks (bubbles, fissures, etc) decrease the real density of the MMM. The density can be corrected by taking into account the N_2 pores to discount their volumes to get the density of the hypothetically defect free components of the mixed matrix membrane ρ_{corr}. These so corrected FFV values are shown in Fig. 9 as well.

We can see in Fig. 9 that in all cases the tendencies coincide, i.e. FFV increases always with the load of the filler. Logically, a correction in density changes the evaluated FFV, giving lower FFV when the van der Waals volumes are used and higher FFV when density is evaluated from the CO_2 adsorption. Nevertheless, there is a good coincidence for all the methods, although in the case of HPA and TR-HPA, the deviations are slightly more significant. These cases show very low CO_2 adsorbed within the narrower pores, what could be attributed, as mentioned, to a possible difficulty to evacuate these pores. This could be correlated with the low permeabilities (and high selectivities) shown by these membranes [18]. This could be due to a better tailoring of the procedures used here to the relatively high permeability membranes. The technique works fine for PAA and TR-PAA membranes. In any case, the comparison of FFV values with CO_2 adsorption and those obtained with the van der

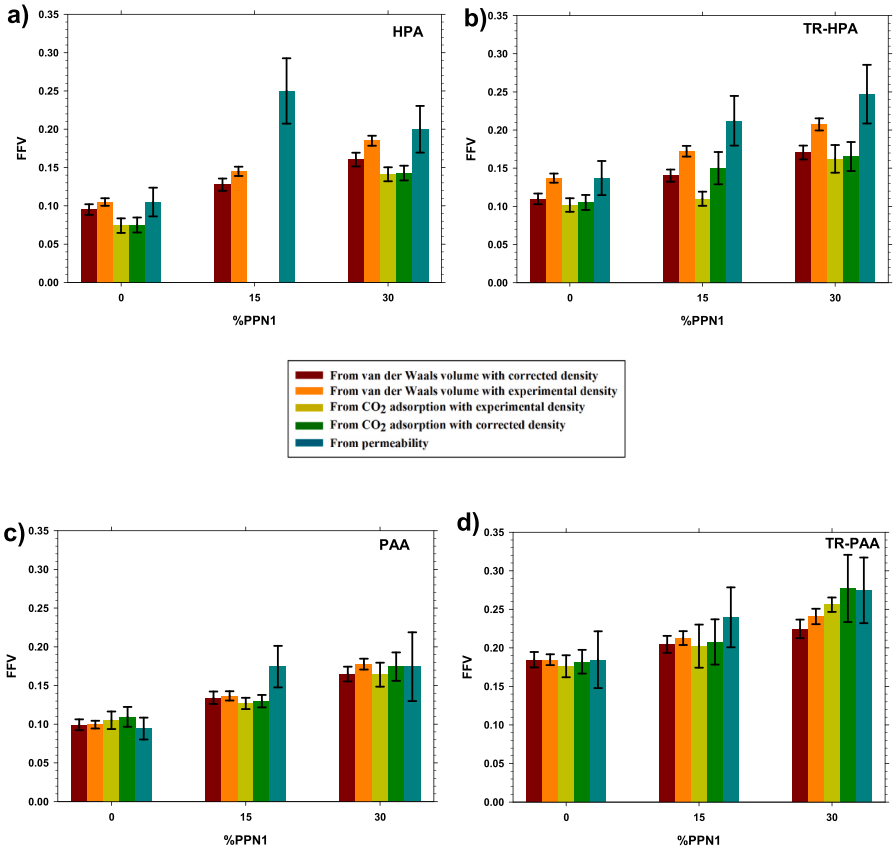

Fig. 9. Comparison of FFV values of the MMMs obtained from CO_2 adsorption with other analyzed methods.

Waals volume, both by using corrected densities, overlap in all cases if the error intervals are taken into account.

When the FFV obtained now are contrasted with those calculated previously by us [18] from permeabilities, we see that those are generally higher (although as can be seen in Fig. 9, its uncertainty is also higher as a consequence of the calculation procedure). This could be reasonable as far as the cracks and fissures within the filler borders and the polymeric matrix should be contributing to permeability even when they give smaller total porous volumes. Moreover, the temperature difference between the permeability measurement (308.15 K) and the adsorption one (273.15 K) contributes to increases this difference. As we have seen from the analysis of adsorption as a function of the temperature, at 308.15 K CO_2 adsorption decreases inside pores with larger size, generating an additional space for Knudsen-type permeation that increases the permeability.

Finally, CO_2 permeability [18] has been correlated with FFV as obtained from CO_2 density corrected by taking into account N_2 adsorption. The corresponding results are shown in Fig. 10.

As should be foreseeable, the increase of FFV due to the presence of PPN1 leads to a corresponding increase in permeability for all the copolymers and both before and after thermal rearrangement in accordance with Eq. (13). It is also clear thermal rearrangement increases permeability as well although this effect is higher for HPA than for PAA. Permeability is proportional to both diffusivity and solubility. Increasing FFV leads mainly to an increase in solubility while diffusivity would be dependent on intersegmental distance for the polymer chains. Therefore, HPAs should increment their intersegmental distance after thermal rearrangement more efficiently than PAAs. In fact, in a recent publication, authors showed, by WAX experiments, that HPAs, both before and after thermal rearrangement, have slightly higher intersegmental distances than PAAs [18]. There, it was also shown, that the selectivity of CO_2 versus other gases could also be explained in terms of FFV. In summary, the consideration of both the intersegmental distance and FFV can explain both the permeability and selectivity of such membranes.

It is worth noting that both, FFV and intersegmental distances, are affected by wide error ranges. Nevertheless, these results are consistent with the evolution of the first CO_2 adsorption peak corresponding to the smallest sizes (see Table 2) that are quite similar to the size of the CO_2 molecule (see Fig. 5).

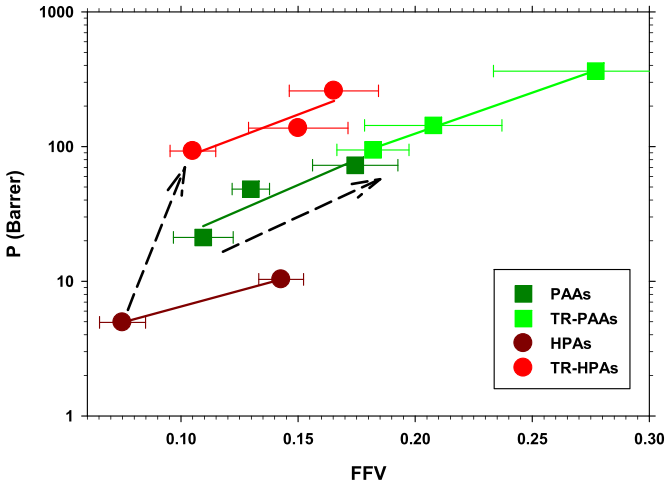

Fig. 10. CO_2 permeability versus FFV from CO_2 adsorption for the 4 families of polymers studied here. Arrows show the effect of thermal rearrangement.

6. Conclusions

A method based on CO_2 adsorption at low pressures allowed us the direct experimental determination of FFV in copolymer families, their thermal treated materials (TR), and their corresponding MMMs by using PPN1 as filler, of this work. The results obtained show a good agreement with the usual methods used to determine this magnitude, which is of great importance in the study of polymer-based membranes for gas permeation. It is foreseeable that the method will apply to other polymer families that show significant CO_2 adsorption at low relative pressures, such as PIMs, other TRs, or other ultrapermeable polymers. It is also probable that the method can be applied more generally by using high-pressure adsorption systems. The acceptable concordance between this CO_2 adsorption method and those based on van der Waals volume determination seems to be because, under these pressure and temperature conditions, CO_2 condenses in pores of the same size as the polymer interchain spaces as considers the Bondi's model employed in molecular simulation.

In the analyzed samples, this method reveals the existence of three groups of pores between 3 and 15 Å, which are the ones that play a significant role in the solution-diffusion gas transport process. The smallest pores (close to the size of the gas molecule) mainly control the diffusion through their bottlenecks modulating the contribution of the polymeric matrix (determined by its intersegmental distance), whereas the other ones are responsible for the solubility of the gas due to condensation capacity by size and affinity. It has been shown that the corresponding FFV can be correlated with CO_2 permeability.

The N_2 adsorption at 77 K has made it possible to determine the pores associated to defects or poor integration of the components and which, due to their size (20–250 Å) should contribute to increasing the permeability by a Knudsen-type mechanism. In addition, the determination of these larger pores, allowed us a correction to the experimental density, to take into account only the effects of the constituent materials.

Declaration of competing interest

The authors declare that they have no known competing financial interests or personal relationships that could have appeared to influence the work reported in this paper.

Data availability

No data was used for the research described in the article.

Acknowledgments

This work was supported by the Spanish Government (AEI) through projects PID2019-109403RB-C21/AEI/10.13039/501100011033 and PID2019-109403RB-C22/AEI/10.13039/501100011033; and by the Regional Government of Castilla y León and the EU-FEDER programme (CL-EI-2021-07, UIC082). C.S acknowledges the Regional Government of Castilla y Leon for her Ph. D. contract.

Appendix A. Supplementary data

Supplementary data to this article can be found online at https://doi.org/10.1016/j.memsci.2023.121841.

References

[1] K. Ghosal, B.D. Freeman, Gas separation using polymer membranes: an overview, Polym. Adv. Technol. 5 (11) (1994) 673–697, https://doi.org/10.1002/pat.1994.220051102.

[2] G. Ji, M. Zhao, Membrane separation technology in carbon capture, in: Y. Yun (Ed.), Recent Advances in Carbon Capture and Storage, IntechOpen, Rijeka, 2017, https://doi.org/10.5772/65723. Ch. 3.

[3] A. Sabetghadam, B. Seoane, D. Keskin, N. Duim, T. Rodenas, S. Shahid, S. Sorribas, C.L. Guillouzer, G. Clet, C. Tellez, M. Daturi, J. Coronas, F. Kapteijn, J. Gascon, Metal organic framework crystals in mixed-matrix membranes: impact of the filler morphology on the gas separation performance, Adv. Funct. Mater. 26 (18) (2016) 3154–3163, https://doi.org/10.1002/adfm.201505352.

[4] E.E. Ünveren, B.Ö. Monkul, Ş. Sarıoğlan, N. Karademir, E. Alper, Solid amine sorbents for CO2 capture by chemical adsorption: a review, Petroleum 3 (1) (2017) 37–50, https://doi.org/10.1016/j.petlm.2016.11.001.

[5] L. Peters, A. Hussain, M. Follmann, T. Melin, M.B. Hägg, CO2 removal from natural gas by employing amine absorption and membrane technology—a technical and economical analysis, Chem. Eng. J. 172 (2) (2011) 952–960, https://doi.org/10.1016/j.cej.2011.07.007.

[6] A. Nuhnen, D. Dietrich, S. Millan, C. Janiak, Role of filler porosity and filler/polymer interface volume in metal–organic framework/polymer mixed-matrix membranes for gas separation, ACS Appl. Mater. Interfaces 10 (39) (2018) 33589–33600, https://doi.org/10.1021/acsami.8b12938.

[7] L.M. Robeson, Polymer membranes for gas separation, Curr. Opin. Solid State Mater. Sci. 4 (6) (1999) 549–552, https://doi.org/10.1016/S1359-0286(00)00014-0.

[8] T. Chen, X. Wei, Z. Chen, D. Morin, S.V. Alvarez, Y. Yoon, Y. Huang, Designing energy-efficient separation membranes: knowledge from nature for a sustainable future, Adv. Membr. 2 (2022), 100031, https://doi.org/10.1016/j.advmem.2022.100031.

[9] C.Z. Liang, T.-S. Chung, J.-Y. Lai, A review of polymeric composite membranes for gas separation and energy production, Prog. Polym. Sci. 97 (2019), 101141, https://doi.org/10.1016/j.progpolymsci.2019.06.001.

[10] C. Aguilar-Lugo, F. Suárez-García, A. Hernández, J.A. Miguel, Á.E. Lozano, J.G. de la Campa, C. Álvarez, New materials for gas separation applications: mixed matrix membranes made from linear polyimides and porous polymer networks having lactam groups, Ind. Eng. Chem. Res. 58 (22) (2019) 9585–9595, https://doi.org/10.1021/acs.iecr.9b01402.

[11] C. Aguilar-Lugo, W.H. Lee, J.A. Miguel, J.G. de la Campa, P. Prádanos, J.Y. Bae, Y. M. Lee, C. Álvarez, Á.E. Lozano, Highly permeable mixed matrix membranes of thermally rearranged polymers and porous polymer networks for gas separations, ACS Appl. Polym. Mater. 3 (10) (2021) 5224–5235, https://doi.org/10.1021/acsapm.1c01012.

[12] C. Soto, E.S. Torres-Cuevas, A. González-Ortega, L. Palacio, P. Prádanos, B. D. Freeman, Á.E. Lozano, A. Hernandez, Hydrogen recovery by mixed matrix membranes made from 6FCl-APAF HPA with different contents of a porous polymer network and their thermal rearrangement, Polymers 13 (24) (2021) 4343, https://doi.org/10.3390/polym13244343.

[13] C. Soto, E.S. Torres-Cuevas, A. González-Ortega, L. Palacio, Á.E. Lozano, B. D. Freeman, P. Prádanos, A. Hernández, Gas separation by mixed matrix membranes with porous organic polymer inclusions within o-hydroxypolyamides containing m-terphenyl moieties, Polymers 13 (6) (2021), https://doi.org/10.3390/polym13060931.

[14] C. Soto, C. Aguilar Lugo, S. Rodríguez, L. Palacio, Á.E. Lozano, P. Prádanos, A. Hernandez, Enhancement of CO2/CH4 permselectivity via thermal rearrangement of mixed matrix membranes made from an o-hydroxy polyamide with an optimal load of a porous polymer network, Separ. Purif. Technol. 247 (2020), 116895, https://doi.org/10.1016/j.seppur.2020.116895.

[15] S. Rico-Martínez, C. Álvarez, A. Hernández, J.A. Miguel, Á.E. Lozano, Mixed Matrix Membranes Loaded with a Porous Organic Polymer Having Bipyridine Moieties, Membranes, 2022.

[16] S.C. Rodrigues, M. Andrade, J. Moffat, F.D. Magalhães, A. Mendes, Carbon membranes with extremely high separation factors and stability, Energy Technol. 7 (4) (2019), 1801089, https://doi.org/10.1002/ente.201801089.

[17] G. Clarizia, Strong and weak points of membrane systems applied to gas separation, Chem. Eng. Trans. 17 (2009) 1675–1680, https://doi.org/10.3303/CET0917280.

[18] C. Soto, B. Comesaña-Gandara, Á. Marcos, P. Cuadrado, L. Palacio, Á.E. Lozano, C. Álvarez, P. Prádanos, A. Hernandez, Thermally rearranged mixed matrix membranes from copoly(o-hydroxyamide)s and copoly(o-hydroxyamide-amide)s with a porous polymer network as a filler—a comparison of their gas separation performances, Membranes 12 (10) (2022) 998.

[19] S. Kim, Y.M. Lee, Rigid and microporous polymers for gas separation membranes, Prog. Polym. Sci. 43 (2015) 1–32, https://doi.org/10.1016/j.progpolymsci.2014.10.005.

[20] S.J.D. Smith, R. Hou, C.H. Lau, K. Konstas, M. Kitchin, G. Dong, J. Lee, W.H. Lee, J. G. Seong, Y.M. Lee, M.R. Hill, Highly permeable thermally rearranged mixed matrix membranes (TR-MMM), J. Membr. Sci. 585 (2019) 260–270, https://doi.org/10.1016/j.memsci.2019.05.046.

[21] H.B. Park, C.H. Jung, Y.M. Lee, A.J. Hill, S.J. Pas, S.T. Mudie, E. Van Wagner, B. D. Freeman, D.J. Cookson, Polymers with cavities tuned for fast selective transport of small molecules and ions, Science 318 (5848) (2007) 254, https://doi.org/10.1126/science.1146744.

[22] B. Comesaña-Gándara, M. Calle, H.J. Jo, A. Hernández, J.G. de la Campa, J. de Abajo, A.E. Lozano, Y.M. Lee, Thermally rearranged polybenzoxazoles membranes with biphenyl moieties: monomer isomeric effect, J. Membr. Sci. 450 (2014) 369–379, https://doi.org/10.1016/j.memsci.2013.09.010.

[23] C.H. Jung, J.E. Lee, S.H. Han, H.B. Park, Y.M. Lee, Highly permeable and selective poly(benzoxazole-co-imide) membranes for gas separation, J. Membr. Sci. 350 (1) (2010) 301–309, https://doi.org/10.1016/j.memsci.2010.01.005.

[24] G. Maier, Gas separation by polymer membranes: beyond the border, Angew. Chem. Int. Ed. 52 (19) (2013) 4982–4984, https://doi.org/10.1002/anie.201302312.

[25] S. Matteucci, Y. Yampolskii, B.D. Freeman, I. Pinnau, Transport of gases and vapors in glassy and rubbery polymers, in: Y. Yampolskii, I. Pinnau, B.D. Freeman (Eds.), Materials Science of Membranes for Gas and Vapor Separation, John Wiley &sons, Berlin, Germany, 2006, pp. 1–47, https://doi.org/10.1002/047002903X.ch1.

[26] D.F. Sanders, Z.P. Smith, R. Guo, L.M. Robeson, J.E. McGrath, D.R. Paul, B. D. Freeman, Energy-efficient polymeric gas separation membranes for a sustainable future: a review, Polymer 54 (18) (2013) 4729–4761, https://doi.org/10.1016/j.polymer.2013.05.075.

[27] M.H. Cohen, D. Turnbull, Molecular transport in liquids and glasses, J. Chem. Phys. 31 (5) (1959) 1164–1169, https://doi.org/10.1063/1.1730566.

[28] J. Chen, M. Longo, A. Fuoco, E. Esposito, M. Monteleone, B. Comesaña Gándara, J. Carolus Jansen, N.B. McKeown, Dibenzomethanopentacene-based polymers of intrinsic microporosity for use in gas-separation membranes, Angew. Chem. Int. Ed. 62 (8) (2023), e202215250, https://doi.org/10.1002/anie.202215250.

[29] W.H. Lee, J.G. Seong, X. Hu, Y.M. Lee, Recent progress in microporous polymers from thermally rearranged polymers and polymers of intrinsic microporosity for membrane gas separation: pushing performance limits and revisiting trade-off lines, J. Polym. Sci. 58 (18) (2020) 2450–2466, https://doi.org/10.1002/pol.20200110.

[30] N. Jusoh, Y.F. Yeong, K.K. Lau, A.M. Shariff, Fabrication of silanated zeolite T/6FDA-durene composite membranes for CO2/CH4 separation, J. Clean. Prod. 166 (2017) 1043–1058, https://doi.org/10.1016/j.jclepro.2017.08.080.

[31] M. Waqas Anjum, F. de Clippel, J. Didden, A. Laeeq Khan, S. Couck, G.V. Baron, J. F.M. Denayer, B.F. Sels, I.F.J. Vankelecom, Polyimide mixed matrix membranes for CO2 separations using carbon–silica nanocomposite fillers, J. Membr. Sci. 495 (2015) 121–129, https://doi.org/10.1016/j.memsci.2015.08.006.

[32] M. Etxeberria-Benavides, O. David, T. Johnson, M.M. Łozińska, A. Orsi, P. A. Wright, S. Mastel, R. Hillenbrand, F. Kapteijn, J. Gascon, High performance mixed matrix membranes (MMMs) composed of ZIF-94 filler and 6FDA-DAM polymer, J. Membr. Sci. 550 (2018) 198–207, https://doi.org/10.1016/j.memsci.2017.12.033.

[33] N.H. Suhaimi, Y.F. Yeong, C.W.M. Ch'ng, N. Jusoh, Tailoring CO2/CH4 separation performance of mixed matrix membranes by using ZIF-8 particles functionalized with different amine groups, Polymers 11 (12) (2019) 2042.

[34] A. Bondi, van der Waals volumes and radii, J. Phys. Chem. 68 (3) (1964) 441–451, https://doi.org/10.1021/j100785a001.

[35] A. Bondi, Physical Properties of Molecular Crystals, Liquids and Glasses, John Wiley & Sons, New York, 1968.

[36] D.W. Van Krevelen, K.T. Nijenhuis, Properties of Polymers. Their Correlation with Chemical Structure; Their Numerical Estimation and Prediction from Additive Group Contributions, fourth ed., Elsevier, New York, 2009.

[37] N.R. Horn, A critical review of free volume and occupied volume calculation methods, J. Membr. Sci. 518 (2016) 289–294, https://doi.org/10.1016/j.memsci.2016.07.014.

[38] M.J.S. Dewar, E.G. Zoebisch, E.F. Healy, J.J.P. Stewart, Development and use of quantum mechanical molecular models. 76. AM1: a new general purpose quantum mechanical molecular model, J. Am. Chem. Soc. 107 (13) (1985) 3902–3909, https://doi.org/10.1021/ja00299a024.

[39] Version 2017R2, BIOVIA Materials Studio, Dassault Systèmes, 2017.

[40] Y.P. Yampolskii, Methods for investigation of the free volume in polymers, Russ. Chem. Rev. 76 (1) (2007) 59, https://doi.org/10.1070/RC2007v076n01ABEH003629.

[41] Y.P. Yampolskii, Fractional free volume, in: E. Drioli, L. Giorno (Eds.), Encyclopedia of Membranes, Springer-Verlag, Berlin, 2016, https://doi.org/10.1007/978-3-662-44324-8.

[42] G. Dlubek, A.P. Clarke, H.M. Fretwell, S.B. Dugdale, M.A. Alam, Positron lifetime studies of free volume hole size distribution in glassy polycarbonate and polystyrene, Phys. Status Solidi(A) 157 (2) (1996) 351–364, https://doi.org/10.1002/pssa.2211570218.

[43] C. Soto, E.S. Torres-Cuevas, L. Palacio, P. Prádanos, B.D. Freeman, Á.E. Lozano, A. Hernández, B. Comesaña-Gándara, Gas permeability, fractional free volume and molecular kinetic diameters: the effect of thermal rearrangement on ortho-hydroxy polyamide membranes loaded with a porous polymer network, Membranes 12 (2) (2022) 200.

[44] A.W. Thornton, K.M. Nairn, A.J. Hill, J.M. Hill, New relation between diffusion and free volume: I. Predicting gas diffusion, J. Membr. Sci. 338 (1) (2009) 29–37, https://doi.org/10.1016/j.memsci.2009.03.053.

[45] J.C. Jansen, M. Macchione, E. Tocci, L. De Lorenzo, Y.P. Yampolskii, O. Sanfirova, V.P. Shantarovich, M. Heuchel, D. Hofmann, E. Drioli, Comparative study of different probing techniques for the analysis of the free volume distribution in amorphous glassy perfluoropolymers, Macromolecules 42 (19) (2009) 7589–7604, https://doi.org/10.1021/ma901244d.

[46] Y.P. Yampolskii, N.E. Kaliuzhnyi, S.G. Durgar'yan, Thermodynamics of sorption in glassy poly(vinyltrimethylsilane), Macromolecules 19 (3) (1986) 846–850, https://doi.org/10.1021/ma00157a062.

[47] G. Golemme, J.B. Nagy, A. Fonseca, C. Algieri, Y. Yampolskii, 129Xe-NMR study of free volume in amorphous perfluorinated polymers: comparsion with other methods, Polymer 44 (17) (2003) 5039–5045, https://doi.org/10.1016/S0032-3861(03)00450-6.

[48] Y.P. Yampolskii, V.P. Shantorovich, F.P. Chernyakovskii, A.I. Kornilov, N.A. Plate, Estimation of free volume in poly(trimethylsilyl propyne) by positron annihilation and electrochromism methods, J. Appl. Polym. Sci. 47 (1) (1993) 85–92, https://doi.org/10.1002/app.1993.070470111.

[49] J.G. Victor, J.M. Torkelson, On measuring the distribution of local free volume in glassy polymers by photochromic and fluorescence techniques, Macromolecules 20 (9) (1987) 2241–2250, https://doi.org/10.1021/ma00175a032.
[50] C. Soto, J. Carmona, B.D. Freeman, L. Palacio, A. González-Ortega, P. Prádanos, Á. E. Lozano, A. Hernandez, Free volume and permeability of mixed matrix membranes made from a terbutil-M-terphenyl polyamide and a porous polymer network, Polymers 14 (15) (2022) 3176.
[51] B. Lopez-Iglesias, F. Suárez-García, C. Aguilar-Lugo, A. González Ortega, C. Bartolomé, J.M. Martínez-Ilarduya, J.G. de la Campa, Á.E. Lozano, C. Álvarez, Microporous polymer networks for carbon capture applications, ACS Appl. Mater. Interfaces 10 (31) (2018) 26195–26205, https://doi.org/10.1021/acsami.8b05854.
[52] S.J. Gregg, K.S.W. Sing, Adsorption, Surface Area, and Porosity, second ed., Academic Press, New York, 1982.
[53] M.M. Dubinin, Fundamentals of the theory of adsorption in micropores of carbon adsorbents: characteristics of their adsorption properties and microporous structures, Carbon 27 (3) (1989) 457–467, https://doi.org/10.1016/0008-6223(89)90078-X.
[54] M.J. Bojan, W.A. Steele, Computer simulation in pores with rectangular cross-sections, Carbon 36 (10) (1998) 1417–1423, https://doi.org/10.1016/S0008-6223(98)00133-X.
[55] J.P. Olivier, Modeling physical adsorption on porous and nonporous solids using density functional theory, J. Porous Mater. 2 (1) (1995) 9–17, https://doi.org/10.1007/BF00486565.
[56] M. Kruk, M. Jaroniec, J. Choma, Comparative analysis of simple and advanced sorption methods for assessment of microporosity in activated carbons, Carbon 36 (10) (1998) 1447–1458, https://doi.org/10.1016/S0008-6223(98)00137-7.
[57] P.I. Ravikovitch, A. Vishnyakov, R. Russo, A.V. Neimark, Unified approach to pore size characterization of microporous carbonaceous materials from N2, Ar, and CO2 adsorption isotherms, Langmuir 16 (5) (2000) 2311–2320, https://doi.org/10.1021/la991011c.
[58] P.I. Ravikovitch, S.C.O. Domhnaill, A.V. Neimark, F. Schueth, K.K. Unger, Capillary hysteresis in nanopores: theoretical and experimental studies of nitrogen adsorption on MCM-41, Langmuir 11 (12) (1995) 4765–4772, https://doi.org/10.1021/la00012a030.
[59] J.D. Weeks, D. Chandler, H.C. Andersen, Role of repulsive forces in determining the equilibrium structure of simple liquids, J. Chem. Phys. 54 (12) (1971) 5237–5247, https://doi.org/10.1063/1.1674820.
[60] P. Tarazona, U.M.B. Marconi, R. Evans, Phase equilibria of fluid interfaces and confined fluids, Mol. Phys. 60 (3) (1987) 573–595, https://doi.org/10.1080/00268978700100381.
[61] P. Tarazona, Free-energy density functional for hard spheres, Phys. Rev. 31 (4) (1985) 2672–2679, https://doi.org/10.1103/PhysRevA.31.2672.
[62] Y. Rosenfeld, M. Schmidt, H. Löwen, P. Tarazona, Fundamental-measure free-energy density functional for hard spheres: dimensional crossover and freezing, Phys. Rev. 55 (4) (1997) 4245–4263, https://doi.org/10.1103/PhysRevE.55.4245.
[63] P.I. Ravikovitch, A. Vishnyakov, A.V. Neimark, Density functional theories and molecular simulations of adsorption and phase transitions in nanopores, Phys. Rev. 64 (1) (2001), 011602, https://doi.org/10.1103/PhysRevE.64.011602.
[64] M.B. Sweatman, N. Quirke, *Handbook of Theoretical and Computational Nanotechnology*, American Scientific Publishers, Stevenson Ranch, CA, 2006.
[65] A.V. Neimark, P.I. Ravikovitch, Calibration of pore volume in adsorption experiments and theoretical models, Langmuir 13 (19) (1997) 5148–5160, https://doi.org/10.1021/la970266s.
[66] D. Cazorla-Amorós, J. Alcañiz-Monge, M.A. de la Casa-Lillo, A. Linares-Solano, CO2 as an adsorptive to characterize carbon molecular sieves and activated carbons, Langmuir 14 (16) (1998) 4589–4596, https://doi.org/10.1021/la980198p.
[67] HyperChem Professional, (Version 8.0.3), Hypercube Inc., 2011.
[68] B. Díez, P. Cuadrado, Á. Marcos-Fernández, J.G. de la Campa, A. Tena, P. Prádanos, L. Palacio, Y.M. Lee, C. Alvarez, Á.E. Lozano, A. Hernández, Thermally rearranged polybenzoxazoles made from poly(ortho-hydroxyamide)s. Characterization and evaluation as gas separation membranes, React. Funct. Polym. 127 (2018) 38–47, https://doi.org/10.1016/j.reactfunctpolym.2018.03.013.
[69] A.F. Ismail, K. Khulbe, T. Matsuura, Gas Separation Membranes: Polymeric and Inorganic, Springer, Berlin, 2015.
[70] H.F. Stoeckli, Microporous carbons and their characterization: the present state of the art, Carbon 28 (1) (1990) 1–6, https://doi.org/10.1016/0008-6223(90)90086-E.
[71] E.P. Barrett, L.G. Joyner, P.P. Halenda, The determination of pore volume and area distributions in porous substances. I. Computations from nitrogen isotherms, J. Am. Chem. Soc. 73 (1) (1951) 373–380, https://doi.org/10.1021/ja01145a126.
[72] D. Shen, M. Bülow, F. Siperstein, M. Engelhard, A.L. Myers, Comparison of experimental techniques for measuring isosteric heat of adsorption, Adsorption 6 (4) (2000) 275–286, https://doi.org/10.1023/A:1026551213604.
[73] NIST Chemistry WebBook, NIST Standard Reference Database Number 69, Eds. P.J. Linstrom and W.G. Mallard, National Institute of Standards and Technology, Gaithersburg MD, 20899.